Payri, R.; Bracho Leon, G.; Marti-Aldaravi, P.; Marco-Gimeno, J. (2021). Mixture Model Approach for the Study of the Inner Flow Dynamics of an AdBlue Dosing System and the Characterization of the Near-Field Spray. SAE International. 1-12. https://doi.org/10.4271/2021-01-0548

Payri, R., Bracho, G., Marti-Aldaravi, P., and Marco-Gimeno, J., "Mixture Model Approach for the Study of the Inner Flow Dynamics of an AdBlue Dosing System and the Characterization of the Near-Field Spray," SAE Technical Paper 2021-01-0548, 2021, doi:10.4271/2021-01-0548

2021-01-0548

Mixture Model approach for the study of the inner flow dynamics of an AdBlue dosing system and the characterization of the near-field spray

Raul Payri, Gabriela Bracho, Pedro Marti-Aldaraví, and Javier Marco-Gimeno
Universitat Politecnica de Valencia

Abstract

Selective Catalytic Reduction stands for an effective methodology for the reduction of NOx emissions from Diesel engines and meeting current and future EURO standards. For it, the injection of Urea Water Solution (UWS) plays a major role in the process of reducing the NOx emissions. A LES approach for turbulence modelling allows to have a description of the physics which is a very useful tool in situations where experiments cannot be performed. The main objective of this study is to predict characteristics of the flow of interest inside the injector as well as spray morphology in the near field of the spray. For it, the nozzle geometry has been reconstructed from X-Ray tomography data, and an Eulerian-Eulerian approach commonly known as Mixture Model has been applied to study the liquid phase of the UWS with a LES approach for turbulence modeling. The injector unit is subjected to typical low-pressure working conditions. The results extracted from it comprise parameters that characterize the hydraulic behavior as well as jet intact length. The conclusions drawn from the model depict differences in the flow behavior between the injector three orifices, with an under-prediction of nozzle and spray characteristics of LES formulation with respect to traditional RANS turbulence treatment.

Introduction

The amount of commercial vehicles with Internal Combustion Engines (ICE) has risen in the last decades. With it, the concern about the emission of pollutants to the atmosphere has followed the same tendency. Some of these emissions mean a problem for the human health as well as for the environment [1]. NOx is one typical product from Diesel engines whose release into the atmosphere needs to be prevented. Selective Catalytic Reduction (SCR) stands for an effective mechanism to reduce these molecules by means of introducing ammonia which decomposes the NOx into diatomic Nitrogen (N_2) and water (H_2O) [2]. Due to safety issues, a mixture of Water and Urea is introduced which will later decompose by means of thermolysis and hydrolysis into NH_3 [3][4][5][6]. The proper distribution of the UWS is of high importance for its later decomposition and a correct NOx reduction.

The needle seat and injector nozzle play an important role in the jet atomization phenomena, but specially on the primary breakup process [7][8][9]. For it, several investigations have been carried on in the literature to understand this phenomenon. Payri et al. [9] analyzed the influence of a conical and cylindrical nozzle on the spray behavior. Vapor penetration was found to be larger for cylindrical nozzles compared with the conical one. In addition, the former nozzle had consistently shorter liquid lengths. Kapusta et al. [10] studied the influence of changing the working fluid of an urea injector from urea to water on global and local spray parameters. For the global parameters, high speed imaging was used, while for the local parameters shadowgraphy technique was employed to visualize an area of 4.5 x 10 mm and obtain the jet angle, droplet size distribution and unbroken liquid length. It showed differences between both working fluids for all the spray parameters. Weber, Reynolds and Ohnesorge were higher for water, but initial velocity and penetration were higher for the UWS. Liquid length for UWS tended to decrease with the injection pressure (first wind induced), while for water the opposite happened (second wind induced). Ishimoto et al. [11] performed a two phase Volume-Of-Fluid (VOF) approach with LES turbulence treatment for a gasoline injector, including coalescence, compressibility and breakup to study the effects of microcavitation in conditions of relatively low injection pressure (4.4 bar) but with a lateral flow in the discharge domain. From the full injector geometry, all the efforts were put into solving the flow out of one hole, which allowed to refine the mesh up to a minimum size of $4\mu m$. They found a correlation between the existence of microcavitation and the zones with high entropy in the region, and after analyzing the size distribution of the droplets, an inhomogeneous distribution was found, which was homogenized when cavitation phenomena appeared. A similar approach is presented by Ling et al. [12], who also couples VOF and Lagrangian Particle Tracking (LPT) by means of a multi-scale model. The bigger particles are resolved within the VOF, while the small droplets are tracked with the LPT. The model is applied to a gas assisted atomizer, showing proper matching of the results in Probability Density Function (PDF) of the scales larger than the grid size, while the smaller ones ae not properly represented. Edelbauer et al. [13] performed another Volume-Of-Fluid simulation on an AdBlue dosing unit, whose purpose was to predict droplet breakup and couple the resulting droplets into an Eulerian-Lagrangian framework. From the three nozzles that composed the unit, only one was simulated to further increase the mesh resolution. Three injection pressures were tested (3, 5 and 9 bar) and the domain was extended downstream long enough to see the breakup. The model could detect droplets with

several shapes and sizes, and the coupling with the Lagrangian tracking method showed good agreement with experimental results. Naik et al. [14] also performed a study on the UWS jet breakup by means of VOF approach with a High Resolution Interface Capturing (HRIC) reconstruction algorithm to evaluate the ligaments formed as a consequence of the primary breakup. Experimental results were shown as well for the CFD to be validated against. Two back-pressure values were simulated (1 and 3 bar) and the approach was accurate to predict spray core length, ligament formation and angle. Additionally, local recirculation was found to be a possible cause of deposit formation. On the other hand, they were not able to predict the secondary breakup because its length scale is much smaller than the minimum cell size used in the simulations.

The aim of this study is to predict the main characteristics of a commercial AdBlue dosing unit using CFD, both the inner flow characteristics and the near-field, analyzing the influence of the injection pressure, and comparing between turbulence modelling techniques available to assess the feasibility of each one of them. Mesh quality and grid requirements for RANS and LES formulation have been assessed by means of a sensitivity study for the first one, and the computation of a quality index for the later one. A secondary objective of this work is the analysis of the performance of each of the orifices that comprise the injector and evaluate whether all of them work in the same way.

The following document is divided in four sections as explained next. The introduction (this section) where the need for this investigation is presented and the state of the art of VOF and Mixture Model simulations for similar applications is commented. The methodology, where the process of geometry obtention and the computational model used for the investigation are explained. Later, the results section, where several analyses are performed, a RANS vs LES comparison, an injection pressure parametric study, an intact length estimation and a breakup assessment. Ending up with the conclusions obtained from the previous results.

Results and discussion

Geometry reconstruction

In order to generate the injector geometry, a computerized tomography (CT)[12][13] of the injector of interest was performed. This procedure is usually performed on a CT machine with a tube source [17]. The spatial resolution achieved for general purpose CT is a compromise between the penetration power and resolution. The tolerance associated with the tomography of this study is of 0.02 mm. From the CT images (Figure 1), the geometry model was generated using a Computer Aided Design (CAD) software. The injector consists of a pentagonal-shaped needle body, which blends into a semi-spherical needle head (Figure 1b and Figure 2). The fluid gets injected into the chamber through three countersunk nozzles with a diameter of 150 µm each that are oriented parallel to the needle axis, and are distributed in a periodic way around the same axis, separated by an arc of 120º each. Needle dynamics were not measured with the CT technique, and after the first simulations of the geometry, the needle lift was set to be a value high enough (0.55 mm) so this component did not act as a flow restriction. The geometrical data that will act as a restrictor therefore will be right upstream of D5 section (Figure 2), of size 0.03mm, and therefore the flow through there will suffer the maximum acceleration, which was already seen in previous studies[18]. The size of this gap is of the order of magnitude of the uncertainty introduced by the CT methodology. For it, an additional study was performed on a specific working condition with several gap dimensions to see which one of them, within the possible range of the CT images, did show the best agreement with the experimental data. With the needle lift set to a constant value, transient behavior of the injector is not going to be studied, but the stationary. The discharge volume where the dosing module injects the UWS has been modeled as a truncated cone whose height is 40 times the nozzle diameter (d_n). The main dimensions of the injector have been summed up in Table 1.

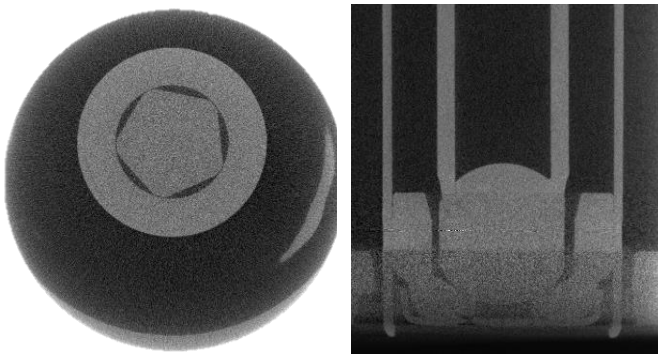

(a) Top view (b) Front view

Figure 1. Injector tomography views.

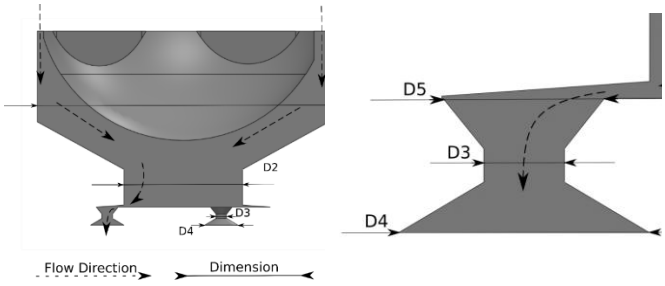

Figure 2.Injector CAD geometry, flow directions and main dimensions (Table 1).

Table 1. Main injector dimensions shown in Figure 2.

Dimension	Value
D1	3.94 mm
D2	1.60 mm
D3	0.15 mm

D4	0.29 mm
D5	0.45 mm

Methodology

Simulations have been performed in the commercial CFD software CONVERGE™ v2.4. Both the gas and liquid phases have been taken into account in a Eulerian-Eulerian framework by using the Mixture Model method. In it, the volumetric Void Fraction of the flow field (which takes the form of Equation 1) is calculated according to the transport properties.

$$\alpha_{phase} = \frac{V_{phase}}{V} \quad (1)$$

Where α_{phase} stands for the volumetric void fraction, V_{phase} indicates the volume of the phase within the cell and V is the total cell volume. The Mixture Model method uses species transport-based formulation, in which the mass fraction of each one of the species is calculated. The transport equation for the mass fraction variables is solved according to Equation 2.

$$\frac{\partial \rho_m}{\partial t} + \frac{\partial \rho_m u_j}{\partial x_j} = \frac{\partial}{\partial x_j}\left(\frac{\rho D \partial Y_m}{\partial x_j}\right) \quad (2)$$

Where ρ_m is the density of the species m, Y_m stands for the mass fraction of species m, and D is the diffusion coefficient. This equation is solved for each of the species present. The void fraction is calculated according to the total mass fractions for the gas and liquid phase obtained with Equation 2 and 3, where the *g* and *l* subscript stand for the gas and liquid species, while n represents the amount of gas species.

$$m_g = \sum_{m=1}^{n} Y_m \quad (3)$$

$$m_l = 1 - m_g \quad (4)$$

Based on these characteristics, the void fraction can finally be calculated according to Equation 5.

$$\alpha = \frac{\frac{m_g}{\rho_g}}{\frac{m_g}{\rho_g} + \frac{m_l}{\rho_l}} \quad (5)$$

The jet breakup and the consequent droplet size distribution are not within the scope of the present work. Therefore, no geometric reconstruction algorithms have been employed. Subsequently, a sharp interface between the gaseous and liquid phases should not be expected. Moreover, in order to simulate a liquid mixture such as the UWS, no reconstruction algorithm could be employed.

The turbulence formulation used for this problem is Large-Eddy-Simulation (LES). This turbulence treatment solves the largest turbulent structures while the smallest ones are modelled. The separation between these structures is done through a low pass filter. This filter is controlled by the grid element size and allows to remove the small structures from the Navier Stokes equation, reducing the computational cost of the method. The Navier-Stokes equations are solved with a Pressure Implicit with Splitting Operator (PISO) algorithm with a tolerance of 1e-03. All the transport equations are solved using a Successive Over Relaxation (SOR) solvers with a tolerance of 1e-04 for the density, energy and species, while for the momentum and pressure, a tolerance of 1e-5 and 1e-8 respectively has been set [19]. The LES sub-grid scale model selected for the work done is Dynamic Smagorinsky [20], a Smagorinsky model modification that allows the model constant C_s to vary in space and time; while the Werner and Wengle model [21] is selected to introduce a Law of the Wall. In addition to the LES methods used; RANS simulations have been applied to the same geometry described. These additional simulations have been done with the same boundary conditions as the LES cases, and the turbulence has been modelled via $k-\varepsilon\ RNG$ equations. Although there is no turbulence treatment capable of properly capturing the effects of the turbulence on the gas-liquid interface, the smearing effect introduced by the species-based solver as well as the lacking of a reconstruction algorithm makes this combination applicable. Additionally, the jet injected is not subjected to a complete atomization regime, but to the first/second wind induced breakup, which implies that the effect of the turbulent behavior will not affect significantly the interface [22]. The corresponding data has been extracted once the case has converged to steady solution. The geometry of the injector requires of a meshing strategy that is capable of resolving larger scales on the discharge volume as well as small gaps within the injector itself. For it, the fluid domain has been discretized into hexahedrals whose characteristic base element size is 150 µm. To be able to cope with the refinement needed for the smaller zones, an octree division of the cells has been done in the regions where needed following the Equation 6. The *p* parameter determines the number of octree divisions applied. The maximum cell reduction is achieved at the smallest gap inside the injector geometry and on the refinement cones introduced at the discharge volume to properly predict the spray behavior once injected, which can be seen in Figure 4.

$$\boldsymbol{L} = \frac{L_{base}}{2^p} \quad (6)$$

The total amount of cells for the LES simulations is of 7.5 million elements, which will be later assessed its quality. For the RANS simulations a mesh sensitivity study is performed. The Mixture Model formulation is known to introduce numerical diffusion in the interface between faces. Therefore, the results that are included in this work should be compared in future studies with other formulations that can deal with the diffusive phenomenon, such as geometry reconstruction routines.

The domain is initialized as follows: the inside of the injector is filled up with a multicomponent liquid phase, which is an Urea-Water Solution (UWS) composed of 32.5% $CO(NH_2)_2$ and 67.5% H_2O in volume, and with the pressure of interest (5, 7 and 9 bar) down to the nozzle throat. The UWS is set to enter the domain at 300 K. The discharge volume is filled with air, and ambient pressure (1bar) and ambient temperature (298 K). The fluid is introduced into the domain with a pressure inlet boundary condition through the upper side of the injector. The fluid leaves the domain through a pressure outlet in the discharge volume (laterals and bottom of the volume) as seen in Figure

3. As the Dynamic Smagorinsky sub-grid model is used, no initialization of the turbulent parameters is needed as the transport closure is done with the C_S^{Δ} constant [23] and not with additional equations.

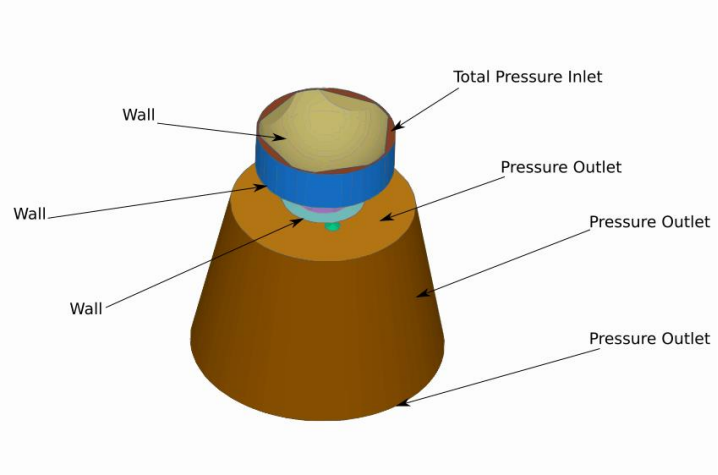

Figure 3. Main boundary conditions of the geometry of interest.

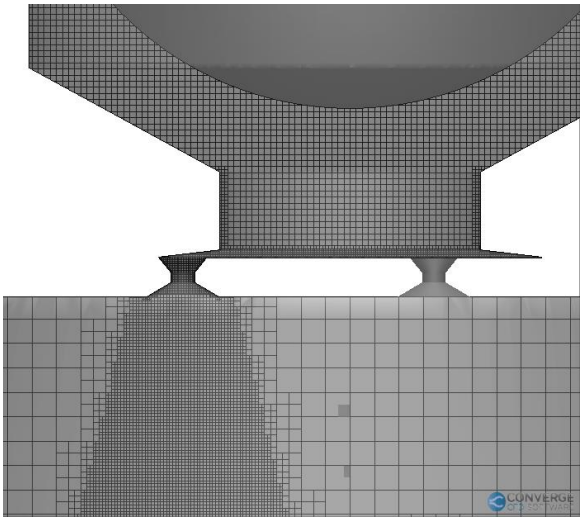

Figure 4. Injector mesh cut through X-Y plane.

As the interest of this study lays on the stationary part of the fluid injection, the initial iterations of the solution have been performed on a coarser mesh in order to speed up the transient fluid dynamics until a steadier solution is achieved. After one convective time of the simulation, the solution has been interpolated into the finer mesh to continue the simulation and achieve better spatial resolution. The mentioned convective time is referred to the time it takes for the fluid to leave the domain at a characteristic velocity.

Reaching stationary conditions is assessed by obtaining the moving average of pressure and Y-velocity at the nozzles and the complete domain, and determining at which point the moving average adopts a steady value (variation < 5%). After that moment is reached, data is collected during 1ms, with a frequency of 1e5 Hz. To obtain the statistical convergence, same fluid variables are collected during certain amount of convective time and have been averaged. This outcome is then compared with the time-averaged results of an increased time window (more temporal data collected). Once variations between time windows fall below 3%, simulations are finished.

Validation

Prior to carrying out the complete analysis, the accuracy of the simulation is tested by comparing the mean values for the urea dosing module extracted from experiments by Payri et al. [24]. As for the simulations, steady state Rate of Injection (ROI) and Rate of Momentum (ROM) data is used. Values are compared to RANS simulations performed at the three injection pressures simulated, at 4 bar (Table 2), 6 bar (Table 3), and 8 bar (Table 4).

Table 2.ROI and ROM results for the experiment [20] and both the RANS and LES simulations for 4 bar of injection pressure, and the error with respect to the experimental output.

	ROI	ROM	ROI Error	ROM Error
Experimental	0.778 g/s	0.0172 N	-	-
RANS	0.725 g/s	0.0112 N	6.81%	34.85%
LES	0.748 g/s	0.0111 N	3.85%	35.45%

Table 3. ROI and ROM results for the experiment [24] and both the RANS and LES simulations for 6 bar of injection pressure, and the error with respect to the experimental output.

	ROI	ROM	ROI Error	ROM Error
Experimental	0.949 g/s	0.026 N	-	-
RANS	0.985 g/s	0,0184 N	3.65%	30%
LES	0.919 g/s	0.0166 N	3.16%	36.15%

Table 4.ROI and ROM results for the experiment [20] and both the RANS and LES simulations for 8 bar of injection pressure, and the error with respect to the experimental output.

	ROI	ROM	ROI Error	ROM Error
Experimental	1.102 g/s	0.0349 N	-	-
RANS	1.085 g/s	0.0256 N	1.54%	27.9%
LES	1.110 g/s	0.0241 N	0.72%	30.94%

The results of this comparison show a good agreement on the flow rate of the computational methods, both RANS and LES with the experimental data shown for the three pressures simulated. On the other hand, the momentum captured is underestimated for all the injection pressures by converge. Similar differences have arisen in other validation studies such as Mohapatra et al. [25] which show ROM differences higher than 10%. Such discrepancies may arise due to not having needle dynamics in the RANS nor LES. A constant

needle lift has been set in the simulations as the experimental lift curve remains unknown. The lift selected has set highly enough to not become a constraint of the flow which could lead to some error. What is more, RANS simulations ($k-\varepsilon\ RNG$ in this case) do not accurately predict flow detachment which will affect the section effective velocity and therefore the momentum. Additionally, the experimental obtention of the momentum value [24] is expected to have considerable uncertainties that also could add some deviation to the results.

RANS Mesh sensitivity study

A mesh sensitivity analysis is done by using four different geometries, Mesh 1, 2, 3 and 4, whose base sizes were modified to coarsen or refine the elements. Results of ROI an ROM have been included in Table 5, as well as the variation between these values of each mesh with respect the immediately coarser mesh. With this data, the mesh with 0.8 million elements is found to be the minimum element number mesh that is capable of properly capturing the orifices mass flow and momentum.

Table 5. ROI and ROM results for the mesh sensitivity study, of the UWS geometry at a working injection pressure of 6 bar (gauge).

Mesh (Nº of Elements)	ROI	ROM	Variation in ROI	Variation in ROM
Mesh 1 (0.6 Million)	1.271 g/s	0.0347 gm/s	-	-
Mesh 2 (0.8 Million)	1.249 g/s	0.0335 gm/s	1.75 %	3.45 %
Mesh 3 (3.3Million)	1.246 g/s	0.0334 gm/s	0.24 %	0.29 %
Mesh 4 (10Million)	1.246 g/s	0.0334 gm/s	0 %	0 %

LES quality study

In order to assess whether if sufficient turbulent scales and enough turbulent energy is resolved in the simulation, a criterion proposed by Pope [26] is introduced. The index of quality stated relies on comparing the resolved turbulent kinetic energy with the total turbulent kinetic energy of the flow field (Equation 7). The resolved part is obtained from the filtered velocity fluctuations (Equation 8), while the modelled part is solved according Equation 9, where ν_{SGS} stands for the sub-grid viscosity, C_m is a constant and Δ_e is the characteristic cell length ($\sqrt[3]{Vol}$). The quality parameter is obtained comparing the amount of resolved kinetic energy from the global turbulent kinetic energy. The sub-grid variables correspond to the turbulent small scales that are filtered out (not resolved) by the grid filter Δ, and therefore need to be modelled. The LES sub-grid models focus on how to solve the sub-grid stress tensor, and then the mentioned sub-grid viscosity. In the particular case of the Dynamic Smagorinsky sub-grid model, a second filtering is applied to calculate the Germano identity [20], later used to obtain the Dynamic Smagorinsky coefficient C_S^{Δ}, and then the stress tensor $\tau_{ij} = -2C_S^{\Delta}|\bar{S}|\overline{S_{ij}}$.

$$IQ_k = \frac{k_{res}}{k_{res}+k_{mod}} \quad (9)$$

$$k_{res} = \frac{1}{2}\left(u_{i,RMS}^2 + u_{j,RMS}^2 + u_{k,RMS}^2\right) \quad (7)$$

$$k_{mod} = \frac{\nu_{SGS}^2}{C_m^2\Delta_e^2} \quad (8)$$

Achieving an IQ > 0.8 (80% of the turbulent kinetic energy resolved) is considered an acceptable value [26]. Figure 5 shows the resulting index for the three orifices of the injector. The previous recommended value is achieved for most of the domain, more importantly in injection regions for the three holes. Low-quality values are achieved in the zones within the injector where no fluctuations are expected (Figure 5), and therefore not having a considerable turbulent kinetic energy to be solved. In the discharge volume, other low-quality zones arise due to having a considerable coarse mesh away from the refinement cone, as well as well-located small sized spots within the jet itself (IQk > 0.5), as seen in Figure 4. In it is also included the velocity magnitude of each of the three sections, where the main low-quality regions of the domain are located where there is almost null velocity or no velocity gradients.

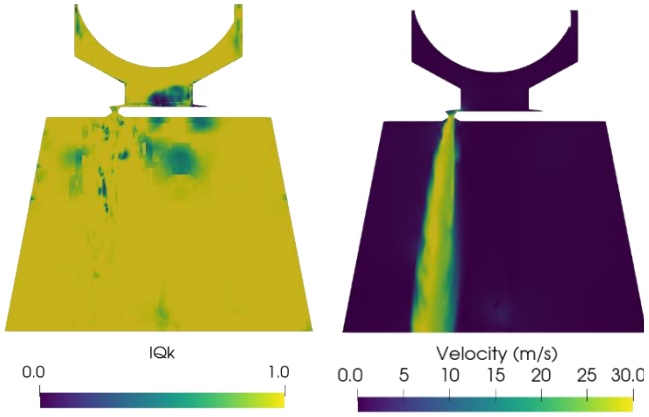

Figure 5. Index of Quality for the first orifice of the injector geometry with the respective velocity contours at an injection pressure of 6 bar.

Flow morphology

An interesting behavior of the current urea dosing module is related to the difference in flow patterns between its three holes. Figure 6 shows how the spray coming out from the second and third hole is different from the first one once the stationary part of the simulation is reached. Orifice 1 shows no significant change in its morphology from the injection into de discharge volume until it leaves it apart from its expansion in the ambient gas. On the other hand, the two other orifices result in similar shapes with respect to each other, showing an oscillatory behavior, from the middle of the discharge volume towards the spray exit on the lower surface. Figure 7 shows the instantaneous velocity contours. The differences between orifices are shown here as well, in addition to differences in velocity magnitude which could be caused by the introduction of numerical

viscosity in the nozzles in which the flow is not perpendicular to the cell faces [27].

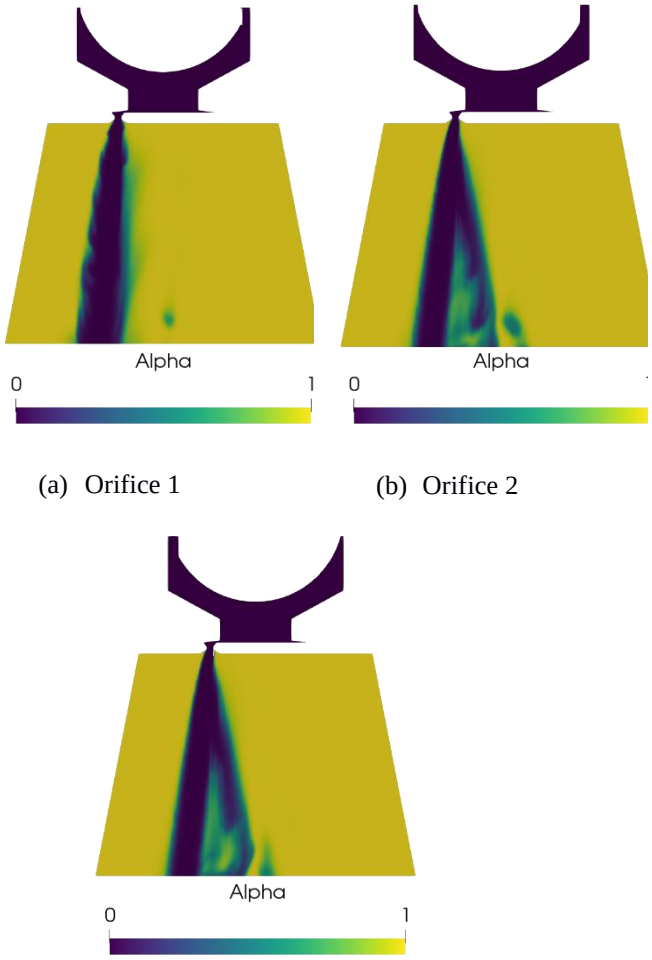

(a) Orifice 1 (b) Orifice 2

(c) Orifice 3

Figure 6. Instantaneous Void Mass Fraction for the three injector orifices.

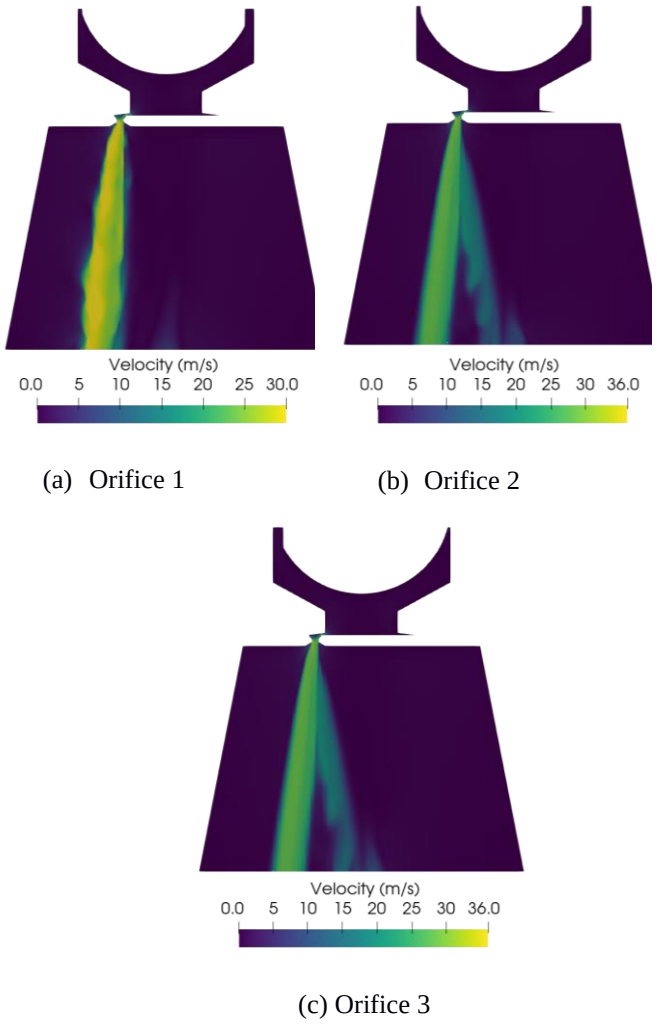

(a) Orifice 1 (b) Orifice 2

(c) Orifice 3

Figure 7. Instantaneous velocity contours for the three injector orifices.

Figure 8 allows to further understand the spray flow near the discharge volume domain. It shows a perpendicular cut to the injector axis at 30D (4.5mm) from the nozzle exit, where D stands for the injector nozzle diameter. It shows that instead of a spray splitting in Orifices 2 and 3, it is an increasing instability of the spray which has induced a wave-shaped oscillation. That answers why in Figure 6 appears ambient gas in between the UWS spray. The first nozzle is clearly differentiated from the other two as the transversal cut shows a rounded shape spray cone.

In order to compare the LES results with the RANS outcomes, the time-averaged fields for the domain have been obtained, and the previous orifices representation is shown in Figure 9. If these snapshots are taken as well from the RANS simulations Figure 10, the first noticeable differences appear. RANS results show identical mass void fraction results for all the three nozzles. If compared with the LES average results, only Orifices 2 and 3 show the flow spread towards the injector axis that is present in Figure 10. On the other hand, the ambient gas gap that lies within the UWS spray is still present. Orifice 1 clearly shows a different distribution, as there is no

such spray spread.

These differences should later be reflected by analyzing individually each one of the orifices of the injector, as the RANS results should show an almost identical performance, while for the LES results, some differences should be seen between the three nozzles depicted.

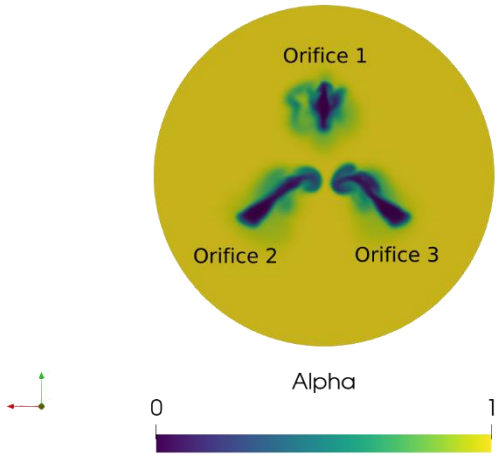

Figure 8. Injector axis perpendicular Void Mass Fraction at 1.6e4 time steps.

To further analyze the nozzle differences, the very same parameters of interest presented at the validation section have been obtained by discretizing the contribution of each nozzle. RANS simulations show slight differences between the mass flow injected and the momentum of the flow. Figure 11 shows how for the three injection pressures simulated, the Orifice 1 shows always lower injection rate and momentum if compared to the remaining other two orifices. On the other hand, Orifices 2 and 3 present an almost identical behavior, which agrees on the different flow topologies presented before. This contributes to the need of performing non-steady simulations to fully capture the flow dynamics of the UWS.

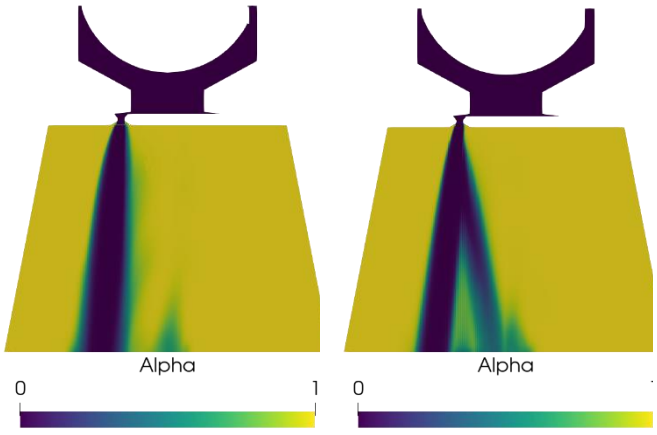

(a) Orifice 1 (b) Orifice 2

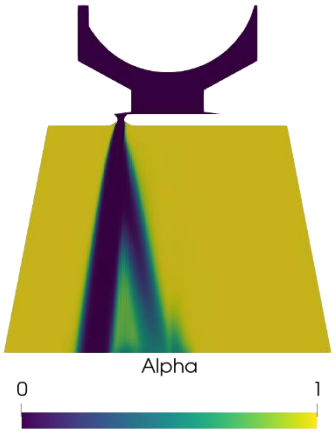

(c) Orifice 3

Figure 9. LES averaged Mass Void Fraction at the three different orifices, at 6 bar injection pressure.

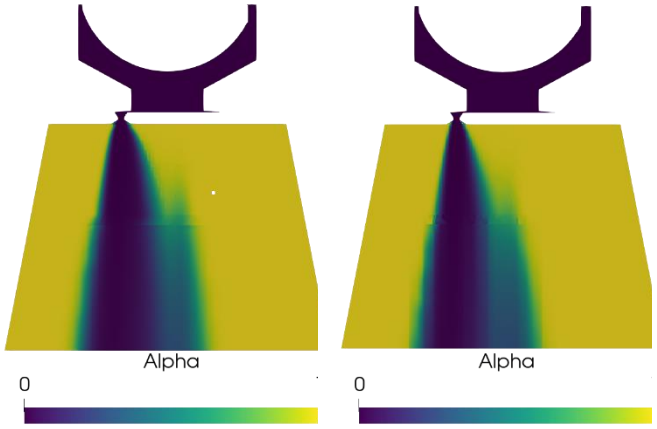

(a) Orifice 1 (b) Orifice 2

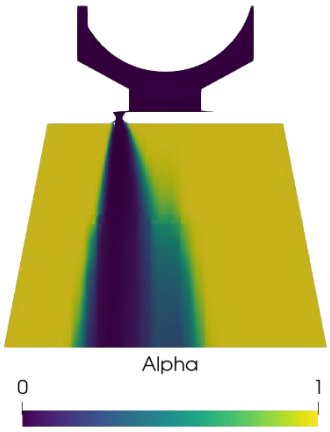

(c) Orifice 3

Figure 10. Void Mass Fraction for the three injector orifices, at 6 bar injection pressure, with RANS $k-\varepsilon$ *RNG* turbulence treatment.

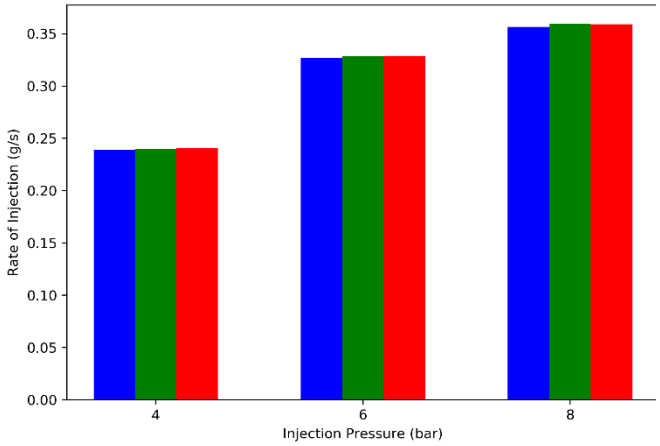

(a) Rate of Injection

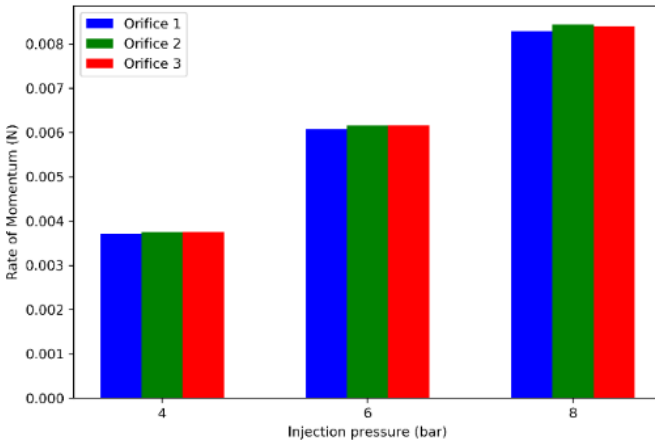

(b) Rate of Momentum

Figure 11. Rate of Injection and Rate of Momentum values for the three orifices and the three injection pressures (4, 6 and 8 bar) for the RANS simulations.

Moreover, streamlines flowing through each of the injector orifices has been plotted in Figure 12 in order to detect where the streamlines differ for each orifice. Each nozzle gets a third part of the working fluid through the inlet, and no remarkable differences can be depicted in this way. Once the fluid gets to the discharge volume, Orifices 2 and 3 spread the spray more than Orifice 1.

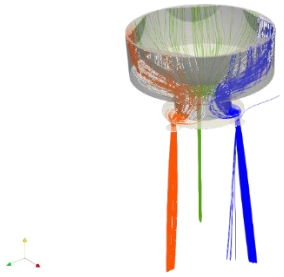

Figure 12. UWS streamlines for each different nozzle. Orange = Orifice 1, Blue = Orifice 2, Green = Orifice 3.

To detect where the differences come from, plots of velocity components at the nozzle exit plane have been extracted, and they have been included in Figure 13, Figure 14 and Figure 15. For the Y component of the velocity field, the three orifices appear to show the same behavior, as the topology of each nozzle seems to be rotated exactly 120º respectively. Differences arise with X and Z component, where Orifices 2 and 3 share the same velocity shape, rotated a third of a circumference as well as in the Y-velocity component (with negative sign for the X due to the position of the origin of the coordinate axis, in the middle of both orifices), but the Orifice 1 shows a different distribution for these two velocity components. It is evident how in the Orifices 2 and 3 there is a strong X and Z component that pushes the fluid towards the injector axis which later

leads to the shapes shown in Figure 6, while on the Orifice 1 a nozzle centered swirling flow shows up, which keeps together the jet core after being injected into the discharge volume.

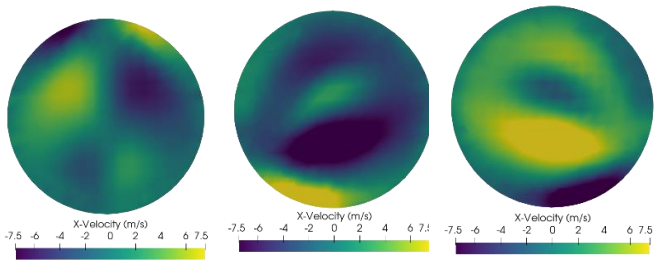

(a) Orifice 1 (b) Orifice 2 (c) Orifice 3

Figure 13. X-Velocity component for the three UWS injector orifices.

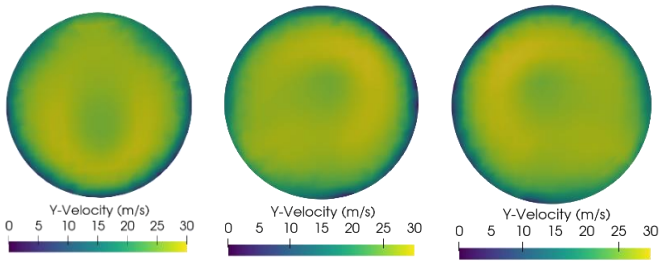

(a) Orifice 1 (b) Orifice 2 (c) Orifice 3

Figure 14. Y-Velocity component for the three UWS injector orifices.

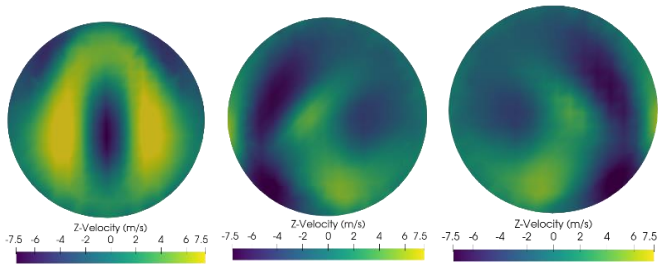

(a) Orifice 1 (b) Orifice 2 (c) Orifice 3

Figure 15. Z-Velocity component for the three UWS injector orifices.

Breakup length

The jet intact length has been calculated for each of the three nozzles. For it, the time average data has been used. The intact length criterion is the 99,9% of the mass void fraction. It is measured from the orifice outlet section. A representative view of the results is included in Figure 16. The corresponding value has been obtained for both computational methodologies, RANS (Figure 17a) and LES (Figure 17b), and for each of the three injection pressures (4, 6 and 8 bar). It is clearly visible that there are notable differences between one of the orifices and the other two, especially in de data coming from the LES simulations. RANS results do not show significant variations of the breakup length when the injection pressure is increased for Orifices 2 and 3.

Results from the LES show differences with respect RANS data, both in the tendency with the pressure and overall values. A clear trend now appears for all the three orifices, decreasing the result with increasing pressure. This decrease in Breakup length helps with the atomization process, as expected. Orifice 1 keeps showing a larger value for all the working injection pressures, and the intact length of the remaining Orifices (2 and 3) show a breakup length higher than 2mm at the lowest injection pressure, which did not happen at the RANS simulations. The trend is similar to experimental results which computed the unbroken liquid length at pressures lower than 4 bar [10], although the values presented there were larger, being the mean unbroken liquid length 6 mm for an injection pressure of 4 bar. As stated previously, Mixture Model method introduces considerable diffusion phenomena to the interface between phases. Furthermore, the intact length criteria introduced was very sensitive to the value chosen, changing the value obtained by the order of 1 mm by choosing a criterion 0.01% higher or lower.

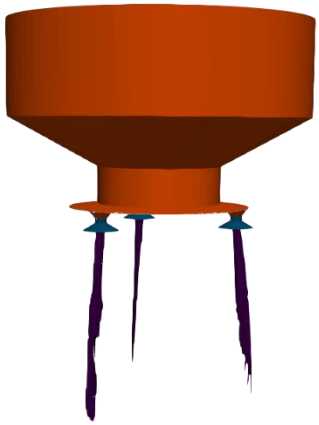

Figure 16. Breakup length representation obtained for the LES, averaged data at 6 bar of injection pressure.

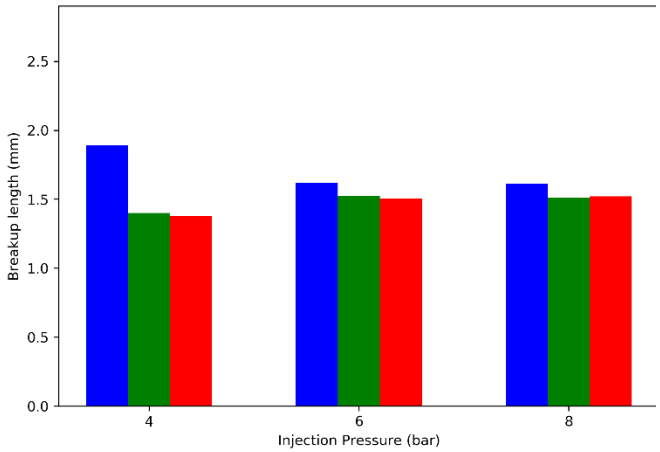

(a) RANS

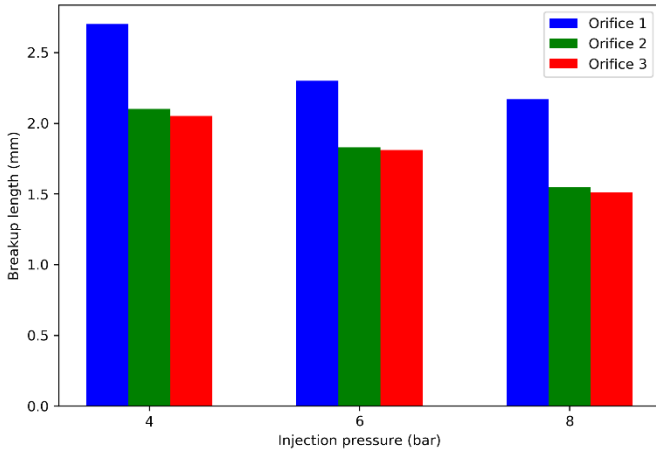

(b) LES

Figure 17. Breakup length of the UWS jet for the three injector orifices and for the three injection pressures, obtained by RANS and LES turbulence treatment.

Additionally, from the flow characteristics at the nozzle exit, it has been plotted into a Reynolds (Re) – Ohnesorge (Oh) diagram in which breakup regime the flow is found. Both numbers have been obtained based on characteristic data extracted at the nozzles from the simulation according to Equation 10 and Equation 11.

$$Re = \frac{\rho u D}{\mu} \quad (10)$$

$$Oh = \frac{\mu}{\sqrt{\rho \sigma D}} \quad (11)$$

The calculated points with the previous formulas fall in the boundary between the 1st wind-induced and 2nd wind-induced regimes (Figure 18). As Figure 19 shows, the breakup length varies with the nozzle velocity, and the trends change accordingly to the regime the flow is working in. The case of an injection pressure of 4 bar lies in the 1st wind induced region, while the remaining injection pressures happen to fall in the 2nd wind induced regime. It must be noted that those boundaries are representative and are not strict limits between one or another regime [28]. Having that into account, it is clear to state that the shortening breakup length of the LES results is a consequence of working on the first regime. Further analysis could be done by testing the injector at higher injection pressures that the ones tested here to allocate when the flow switches to the 2nd wind regime.

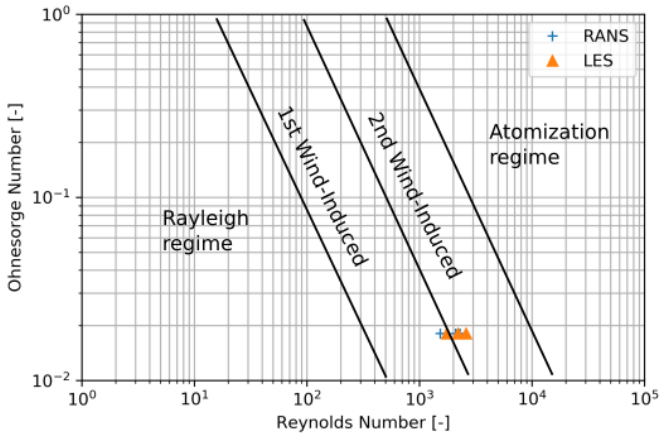

Figure 18. Ohnesorge-Reynolds diagram for the flow characteristics at the nozzle exit for the 4, 6 and 8 bar of injection pressure, for RANS and LES simulations.

Comparing the breakup lengths obtained in Figure 17b with Root Mean Square values of the velocity obtained in the LES outputs, a qualitative correlation was found for Orifices 2 and 3. RMS values are presented in Figure 20. RMS contour in the mentioned nozzles have an expansion in both spray sides and reach a peak of 7.5 m/s in RMS magnitude when the spray has theoretically break up into droplets and ligaments according to the lengths obtained with the 99.9% criteria. Prior to this point, RMS increases progressively as the jet starts to disintegrate.

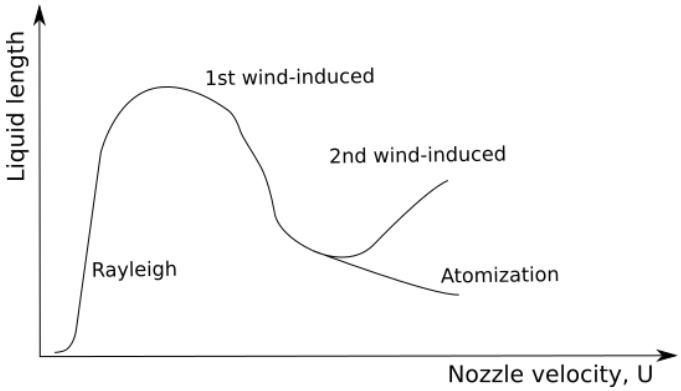

Figure 19. Breakup length evolution with the nozzle exit velocity, according

to [29].

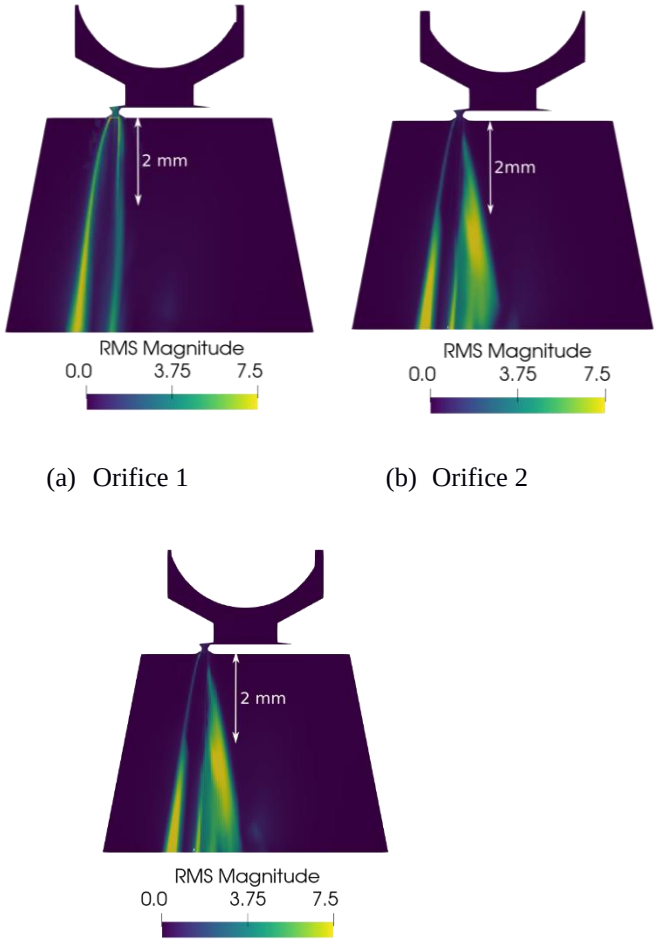

(a) Orifice 1 (b) Orifice 2

(c) Orifice 3

Figure 20. Velocity RMS contours of the three orifices for a pressure injection of 6 bar.

Conclusions

In the work presented, the geometry of an UWS injector has been created from CT data to simulate the inner flow dynamics and near-field spray characteristics using a Mixture Model approach and LES turbulence modelling. The results have been validated against RANS data obtained from the same geometry, as well as experimental data. Results on ROI and ROM for each injector nozzle has been obtained performing a parametric study over the injectors operating range. From the outcomes obtained, the following conclusions could be drawn:

- The proposed CFD methodology prediction on ROI for the injector is accurate if compared with experiments. LES shows a maximum deviation of a 3.8% for a specific injection pressure of 4 bar, and it decreases as higher injection pressures are simulated. ROM on the other hand is not properly captured and underpredicts the experimental results, both in RANS and LES turbulence treatment.
- CT spatial resolution needed for this application needs to be high enough to properly characterize the UWS injector geometry. In this study, as it was not sufficient, a simulation RANS campaign was launched iterating on size of the narrowest gap within the injector, in which the tomography showed high uncertainty, to match ROI experimental data.
- Injector behavior appears to be different between one of the orifices and the two remaining in the LES simulations. Injection rate and momentum are slightly lower for the different orifice compared to the two that behave equally. Mass void fraction contours clearly exhibit differences in the jet behavior once the flow enters the discharge volume. No strong evidence was found with a streamline study. Further analysis needs to be made to assess the cause.
- CFD can predict jet intact length, exhibiting results of the same order of magnitude as experimental data from literature. For a feasible comparison, intact length experimental results performed on the same injection pressure conditions should be obtained.
- Intact length varies with injection pressure, but the working conditions the injector has been subjected to does not give a clear idea on which breakup regime the spray is under. LES results suggest the analyzed operating conditions fall in the 1st wind induced regime for the monotonically decreasing lengths. The Re-Oh chart shows plausible results according to the LES trend found.
- Qualitative correlation of the velocity RMS and intact length calculations (99.9% criterion) was found. Maximum RMS values occurred right after the jet has disintegrated into droplets and ligaments, and the RMS monotonically increases up to this point. After the flow reaches the breakup length, the RMS contours expand as well.
- General Mixture Model approaches introduces numerical diffusion on the gas-liquid interface. In future work, the use of a surface reconstruction algorithm may increase the precision of the results.
- No droplet formation was detected. Additional refinement should be done on the mesh, whose minimum cell size shall be the minimum droplet diameter to be detected. Present work introduces minimum cell size of 22 µm, and other works showed a considerable number of droplets found below that value [18].

Further studies should be carried out to identify the cause of the different orifice morphology. A possible reason behind it might be

the influence of the orientation of the injector nozzles with respect to the cartesian mesh that might be introducing numerical viscosity and affect the solution. Additionally, in order to predict droplet breakup, the use of a PLIC algorithm would be needed, as well as considerable mesh refinement should be performed on a section of the injector introduced to make the simulation feasible when it comes to cell count.

References

[1] R. D. Reitz *et al.*, "IJER editorial: The future of the internal combustion engine," *Int. J. Engine Res.*, vol. 21, no. 1, p. 146808741987799, 2019, doi: 10.1177/1468087419877990.

[2] R. van Helden, R. Verbeek, F. Willems, and R. van der Welle, "Optimization of Urea SCR deNOx Systems for HD Diesel Engines," Mar. 2004, doi: https://doi.org/10.4271/2004-01-0154.

[3] G. Zheng, A. Fila, A. Kotrba, and R. Floyd, "Investigation of Urea Deposits in Urea SCR Systems for Medium and Heavy Duty Trucks," Oct. 2010, doi: https://doi.org/10.4271/2010-01-1941.

[4] S. D. Yim *et al.*, "Decomposition of urea into NH3 for the SCR process," *Ind. Eng. Chem. Res.*, vol. 43, no. 16, pp. 4856–4863, 2004, doi: 10.1021/ie034052j.

[5] R. Hartley, C. Henry, S. Eakle, and Z. Tonzetich, "Deposit Reduction in SCR Aftertreatment Systems by Addition of Ti-Based Coordination Complex to UWS," 2019, doi: https://doi.org/10.4271/2019-01-0313.

[6] J. Han, J. Lee, Y. Oh, G. Cho, and H. Kim, "Effect of UWS injection at low exhaust gas temperature on NOx removal efficiency of diesel engine," *Int. J. Automot. Technol.*, vol. 18, no. 6, pp. 951–957, 2017, doi: 10.1007/s12239-017-0093-6.

[7] M. Bode, F. Diewald, D. O. Broll, J. F. Heyse, V. Le Chenadec, and H. Pitsch, "Influence of the Injector Geometry on Primary Breakup in Diesel Injector Systems," 2014, doi: https://doi.org/10.4271/2014-01-1427.

[8] R. Payri, J. P. Viera, V. Gopalakrishnan, and P. G. Szymkowicz, "The effect of nozzle geometry over internal flow and spray formation for three different fuels," *Fuel*, vol. 183, pp. 20–33, 2016, doi: https://doi.org/10.1016/j.fuel.2016.06.041.

[9] R. Payri, J. P. Viera, V. Gopalakrishnan, and P. G. Szymkowicz, "The effect of nozzle geometry over the evaporative spray formation for three different fuels," *Fuel*, vol. 188, pp. 645–660, 2017, doi: 10.1016/j.fuel.2016.06.041.

[10] Ł. J. Kapusta, M. Sutkowski, M. Rogóż Rafałand Zommara, and A. Teodorczyk, "Characteristics of water and urea-water solution sprays," *Catalysts*, vol. 9, no. 750, p. 750, 2019, doi: 10.3390/catal9090750.

[11] J. Ishimoto, F. Sato, and G. Sato, "Computational prediction of the effect of microcavitation on an atomization mechanism in a gasoline injector nozzle," *J. Eng. Gas Turbines Power*, vol. 132, no. 8, Aug. 2010, doi: 10.1115/1.4000264.

[12] Y. Ling, S. Zaleski, and R. Scardovelli, "Multiscale simulation of atomization with small droplets represented by a Lagrangian point-particle model," *Int. J. Multiph. Flow*, vol. 76, pp. 122–143, 2015, doi: https://doi.org/10.1016/j.ijmultiphaseflow.2015.07.002.

[13] W. Edelbauer, P. Kolar, D. Schellander, Z. Pavlovic, and R. Almbauer, "Numerical simulation of spray break-up from cavitating nozzle flow by combined Eulerian-Eulerian and Volume-of-Fluid Methods," *Int. J. Comput. Methods Exp. Meas.*, vol. 6, no. 2, pp. 314–325, 2018, doi: 10.2495/CMEM-V6-N2-314-325.

[14] A. Naik, M. Höltermann, E. Lauer, S. Blodig, and F. Dinkelacker, "Modeling of air-assisted spray breakup of urea-water solution using a volume-of-fluid method," *At. Sprays*, vol. 29, no. 6, pp. 553–576, 2019, doi: 10.1615/AtomizSpr.2019030987.

[15] A. C. K. M. Slaney, *Principles of Computerized Tomographic Imaging*. New York, NY: IEEE Press, 1988.

[16] D. J. Duke *et al.*, "High-Resolution X-Ray and Neutron Computed Tomography of an Engine Combustion Network Spray G Gasoline Injector," *SAE Int. J. Fuels Lubr.*, vol. 10, no. 2, pp. 328–343, 2017, doi: 10.4271/2017-01-0824.

[17] B. T. M., *Computed Tomography*. Heidelberg, Germany: Springer Science & Business Media, 2008.

[18] R. Payri, G. Bracho, P. Martí-Aldaraví, and J. Marco-Gimeno, "Computational Study of Urea–Water Solution Sprays for the Analysis of the Injection Process in SCR-like Conditions," *Ind. Eng. Chem. Res.*, vol. 59, no. 41, pp. 18659–18673, Oct. 2020, doi: 10.1021/acs.iecr.0c02494.

[19] Convergent Science, Ed., *CONVERGE 2.4 Manual*. Middleton, 2017.

[20] M. Germano, U. Piomelli, P. Moin, and W. H. Cabot, "A dynamic subgrid-scale eddy viscosity model," *Phys. Fluids A Fluid Dyn.*, vol. 3, no. 7, pp. 1760–1765, Jul. 1991, doi: 10.1063/1.857955.

[21] H. Werner and H. Wengle, "Large-Eddy Simulation of Turbulent Flow Over and Around a Cube in a Plate Channel BT - Turbulent Shear Flows 8," 1993, pp. 155–168.

[22] A. Balabel, "Numerical modeling of turbulence-induced interfacial instability in two-phase flow with moving interface," *Appl. Math. Model.*, vol. 36, no. 8, pp. 3593–

3611, 2012, doi: https://doi.org/10.1016/j.apm.2011.11.006.

[23] J. Kleissl, V. Kumar, C. Meneveau, and M. B. Parlange, "Numerical study of dynamic Smagorinsky models in large-eddy simulation of the atmospheric boundary layer: Validation in stable and unstable conditions," *Water Resour. Res.*, vol. 42, no. 6, Jun. 2006, doi: 10.1029/2005WR004685.

[24] R. Payri, G. Bracho, J. Gimeno, and A. Moreno, "A Methodology for the hydraulic characterization of a Urea-Water Solution injector by means of Spray Momentum Measurement," in *29th European Conference on Liquid Atomization and Spray Systems*, 2019, no. 2-4 September.

[25] C. K. Mohapatra *et al.*, "Collaborative investigation of the internal flow and near-nozzle flow of an eight-hole gasoline injector (Engine Combustion Network Spray G)," *Int. J. Engine Res.*, p. 1468087420918449, Jun. 2020, doi: 10.1177/1468087420918449.

[26] S. B. Pope, "Ten questions concerning the large-eddy simulation of turbulent flows," *New J. Phys.*, vol. 6, p. 35, 2004, doi: 10.1088/1367-2630/6/1/035.

[27] V. S. V. Patankar, "Numerical heat transfer and fluid flow. Von S. V. Patankar. Hemisphere Publishing Corporation, Washington – New York – London. McGraw Hill Book Company, New York 1980. 1. Aufl., 197 S., 76 Abb., geb., DM 71,90," *Chemie Ing. Tech.*, vol. 53, no. 3, p. 225, 1981, doi: https://doi.org/10.1002/cite.330530323.

[28] A. H. Lefebvre and V. G. McDonell, *Atomization and sprays*, Second. Boca Raton, FL: Press, CRC, 2017.

[29] S. P. Lin and R. D. Reitz, "DROP AND SPRAY FORMATION FROM A LIQUID JET," *Annu. Rev. Fluid Mech.*, vol. 30, no. 1, pp. 85–105, Jan. 1998, doi: 10.1146/annurev.fluid.30.1.85.

Contact Information

Pedro Martí-Aldaraví

CMT - Motores Térmicos, Universitat Politècnica de València

Edificio 6D, 46022, Valencia

pedmar15@mot.upv.es

Acknowledgments

The presented work is funded by a grant of Generalitat Valenciana, with reference ACIF/2020/259 and of the European Union. Partial funding comes as well from Spanish Ministerio de Ciencia, Innovación y Universidades through project RTI2018-099706-B-100. Additionally, the experimental hard-ware was purchased through FEDER and Generalitat Valenciana under project IDIFEDER/2018/037.

Definitions/Abbreviations

CAD	Computer Aided Design
CFD	Computational Fluid Dynamics
CT	Computerized Tomography
HRIC	High Resolution Interface Capturing
LES	Large Eddy Simulation
PLIC	Piecewise linear interface calculation
RANS	Reynolds-Averaged Navier-Stokes
RMS	Root Mean Square
ROI	Rate of Injection
ROM	Rate of Momentum
SGS	Sub-Grid Scale
UWS	Urea Water Solution
VOF	Volume-Of-Fluid